The elevation of circulating fibroblast growth factor 23 without kidney disease does not increase cardiovascular disease risk

Eva-Maria Pastor-Arroyo[1], Nicole Gehring[1], Christiane Krudewig[2], Sarah Costantino[3], Carla Bettoni[1], Thomas Knöpfel[1], Sibylle Sabrautzki[4,5], Bettina Lorenz-Depiereux[6], Johanne Pastor[7], Tim M. Strom[6,8], Martin Hrabě de Angelis[4,9,10], Giovanni G. Camici[3], Francesco Paneni[3], Carsten A. Wagner[1] and Isabel Rubio-Aliaga[1]

[1]*Institute of Physiology, University of Zurich, and National Center for Competence in Research NCCR Kidney.CH, Zurich, Switzerland;* [2]*Laboratory for Animal Model Pathology (LAMP), Institute of Veterinary Pathology, Vetsuisse Faculty, University of Zurich, Zurich, Switzerland;* [3]*Center for Molecular Cardiology, University of Zurich, and University Heart Center, Department of Cardiology, University Hospital Zurich, Zurich, Switzerland;* [4]*Institute of Experimental Genetics and German Mouse Clinic, Helmholtz Zentrum München, German Research Center for Environmental Health, Neuherberg, Germany;* [5]*Research Unit Comparative Medicine, Helmholtz Zentrum München, German Research Center for Environmental Health, Neuherberg, Germany;* [6]*Institute of Human Genetics, Helmholtz Zentrum München, German Research Center for Environmental Health, Neuherberg, Germany;* [7]*University of Texas Southwestern Medical Center, Dallas, Texas, USA;* [8]*Institut für Humangenetik, Klinikum rechts der Isar der Technischen Universität München, München, Germany;* [9]*Lehrstuhl für Experimentelle Genetik, Technische Universität München, Freising-Weihenstephan, Germany; and* [10]*Member of German Center for Diabetes Research, Neuherberg, Germany*

High circulating fibroblast growth factor 23 (FGF23) levels are probably a major risk factor for cardiovascular disease in chronic kidney disease. FGF23 interacts with the receptor FGFR4 in cardiomyocytes inducing left ventricular hypertrophy. Moreover, in the liver FGF23 via FGFR4 increases the risk of inflammation which is also found in chronic kidney disease. In contrast, X-linked hypophosphatemia is characterized by high FGF23 circulating levels due to loss of function mutations of the phosphate-regulating gene with homologies to an endopeptidase on the X chromosome (*PHEX*), but is not characterized by high cardiovascular morbidity. Here we used a novel murine X-linked hypophosphatemia model, the *Phex*^{C733RMhda} mouse line, bearing an amino acid substitution (p.Cys733Arg) to test whether high circulating FGF23 in the absence of renal injury would trigger cardiovascular disease. As X-linked hypophosphatemia patient mimics, these mice show high FGF23 levels, hypophosphatemia, normocalcemia, and low/normal vitamin D levels. Moreover, these mice show hyperparathyroidism and low circulating soluble αKlotho levels. At the age of 27 weeks we found no left ventricular hypertrophy and no alteration of cardiac function as assessed by echocardiography. These mice also showed no activation of the calcineurin/NFAT pathway in heart and liver and no tissue and systemic signs of inflammation. Importantly, blood pressure, glomerular filtration rate and urea clearance were similar between genotypes. Thus, the presence of high circulating FGF23 levels alone in the absence of renal impairment and normal/high phosphate levels is not sufficient to cause cardiovascular disease.

Kidney International (2018) ■, ■–■; https://doi.org/10.1016/j.kint.2018.02.017

KEYWORDS: cardiovascular disease; chronic kidney disease; FGF23; phosphate

End-stage renal disease (ESRD), chronic kidney disease (CKD), and also reduced renal function increase the risk of mortality and cardiovascular disease.[1] Left ventricular hypertrophy (LVH) is likely the primary manifestation of uremic cardiomyopathy.[2] LVH affects approximately 70% of patients during intermediate stages of CKD[3] compared with 16% to 21% affected individuals in the general population.[4] CKD patients show high circulating fibroblast growth factor 23 (FGF23), which likely participates in the pathogenesis of left ventricular hypertrophy in these patients.[5] FGF23 together with parathyroid hormone (PTH) and 1,25$(OH)_2$ vitamin D (1,25$(OH)_2$D) is responsible for the regulation of phosphate homeostasis in the organism.[6] FGF23 is synthetized in bone, and after posttranslational modification the active form is secreted into circulation. The action of FGF23 is mediated by coupling to a fibroblast growth factor receptor (FGFR) in the target cell or organ. At least in kidney the presence of the coreceptor αKlotho is required for an effective

Correspondence: *Isabel Rubio-Aliaga, Institute of Physiology, University of Zurich, and the National Center for Competence in Research NCCR Kidney.CH, Winterthurerstrasse 190, 8057 Zurich, Switzerland. E-mail: isabel.rubioaliaga@uzh.ch; or Carsten A. Wagner, Institute of Physiology, University of Zurich, and the National Center for Competence in Research NCCR Kidney.CH, Winterthurerstrasse 190, 8057 Zurich, Switzerland. E-mail: Wagnerca@access.uzh.ch*

Received 10 May 2017; revised 24 January 2018; accepted 1 February 2018

FGF23-FGFR binding.[7] αKlotho is also present in the circulation as soluble Klotho. Its function is still not fully understood, but together with the other major endocrine regulators of phosphate homeostasis, its levels are altered in CKD: FGF23 and PTH are elevated already in the first phases of CKD, whereas soluble Klotho and $1,25(OH)_2D$ are decreased. Phosphate increases in plasma only in later stages of CKD.[8] FGF23 has been suggested as the inductor of left ventricular hypertrophy in chronic kidney disease, by binding to FGFR4 in myocytes in the absence of αKlotho.[5,9] Other authors suggest that αKlotho and phosphate rather than FGF23, PTH, and $1,25(OH)_2D$ levels correlate with the appearance of cardiac hypertrophy and fibrosis.[10] Therefore, we wanted to test in an X-linked hypophosphatemia (XLH) mouse model that has chronic high circulating FGF23 levels whether these animals have a higher risk of cardiovascular disease. Of note, FGF23 levels in XLH are comparable to levels in CKD.[11,12]

XLH (OMIM 307800) is the most common form of hereditary rickets affecting 1 in 20,000 individuals.[13,14] The main feature of this disease is high circulating levels of the hormone FGF23, which lead to hypophosphatemia due to decreased renal phosphate reabsorption. Affected individuals frequently present with bone pain, lower limb deformity, dental anomalies, and muscular symptoms, although the severity grade varies greatly between individuals and between relatives. XLH is caused by mutations in the phosphate-regulating gene with homologies to endopeptidases on the X chromosome (PHEX).[15] The exact physiological function of PHEX is still unknown, but mutations in this gene lead to high synthesis of FGF23 in the bone and secretion to the circulation. A large variety of mutations have been identified in the *PHEX* gene.[16] These mutations include large and small deletions, insertions, nonsense, missense, and splice site mutations. Several XLH mouse models are available.[17,18] The most used mouse XLH model is the Hyp mouse.[19] We have recently reported 2 new mouse XLH models, C3Heb/FeJ-PhexBAP012, and C3Heb/FeJ-PhexBAP024 ($Phex^{C733RMhda}$).[20] $Phex^{C733R}$ mice have a missense mutation in the cysteine at position 733 causing a change to an arginine residue. This mutation has also been described in 2 patients causing a change to a serine residue or a stop codon,[16,21] respectively. Here, we show that these mice are a good XLH model. Second, as the CVD risk increases with age we studied the effect of the primary elevation of FGF23 levels in plasma on indicators of CVD and systemic inflammation in 27-week-old $Phex^{C733R}$ mice.

RESULTS

The $Phex^{C773R}$ mouse line is an XLH model showing primary high FGF23 blood levels

First we analyzed whether hemizygous $Phex^{C733R/Y}$ males and heterozygous $Phex^{C733R/+}$ females showed the typical features of XLH patients. Indeed, $Phex^{C733R/Y}$ males and $Phex^{C733R/+}$ females had high circulating intact FGF23 levels at 12 and 27 weeks of age (Figure 1a; Supplementary Figures S1A and S2A and B). C-terminal FGF23 levels were higher than intact FGF23 levels and also elevated in $Phex^{C733R/Y}$ males when compared with wild-type animals (Supplementary Figure S2C). Moreover, $Phex^{C733R/Y}$ males and $Phex^{C733R/+}$ females were hypophosphatemic and normocalcemic (Figure 1b and c; Supplementary Figures S1B and C and 2D–G). Only female $Phex^{C733R/+}$ showed the hyperphosphaturia detected in XLH patients, whereas $Phex^{C733R/Y}$ males were normophosphaturic (Figure 1d and e). This is probably because male $Phex^{C733R/Y}$ excreted less urine and had higher urine creatinine levels (Supplementary Table S2). The hyperphosphaturia observed in XLH patients is due to downregulation of the sodium-phosphate transporter NaPi-IIa (Slc34a1) protein expression in the proximal tubule provoked by high FGF23 levels in blood. $Phex^{C733R/Y}$ males and $Phex^{C733R/+}$ females showed also clearly reduced NaPi-IIa protein expression in renal brush border membranes (Figure 1g and i; Supplementary Figure S1D and E). $Phex^{C733R/Y}$ males and $Phex^{C733R/+}$ females showed a tendency to hypocalciuria ($P = 0.09$ and 0.07, respectively; Figure 1f and Supplementary Figure S1F). Next, we observed that the protein renal expression of the coreceptor αKlotho was lower in $Phex^{C733R/Y}$ males (Figure 1h and j). Plasma soluble αKlotho was also decreased in $Phex^{C733R/Y}$ males (Figure 1k). XLH patients show abnormally low to normal $1,25(OH)_2D$ levels when considering their hypophosphatemic state.[14] $Phex^{C733R/Y}$ males also showed low $1,25(OH)_2D$ levels (Figure 1l), due to decreased synthesis rate and despite increased inactivation (Supplementary Figure S3A–C). Inactivation and synthesis of $1,25(OH)_2D$ levels is mediated by the renal enzyme 24-hydroxylase (Cyp24a1) and 1α-hydroxylase (Cyp27b1), respectively. Female $Phex^{C733R/+}$ had similar $1,25(OH)_2D$ levels as their wild-type littermates (Figure 1m). Despite the high FGF23 levels in blood, *Cyp27b1* mRNA expression and Cyp24a1 protein expression were similar between wild-type and $Phex^{C733R/+}$ females (Supplementary Figure S3D–F). Hyperparathyroidism is mostly seen in XLH patients treated with phosphate supplements, but has also been reported in untreated XLH patients.[22] $Phex^{C733R/Y}$ males and $Phex^{C733R/+}$ females also presented with higher PTH levels in plasma than their wild-type littermates (Figure 1n; Supplementary Figure S1G). Finally, the $Phex^{C733R}$ mouse line showed as XLH patients alterations in their bone structure and bone mineral density. $Phex^{C733R}$ mice had lower bone mineral density and lower cortical bone mineral density[14,23] (Figure 1o and p; Supplementary Table S3). In conclusion, the $Phex^{C733R}$ mouse line shows a phenotype resembling XLH patients with very high FGF23 levels.

$Phex^{C773R}$ mice have normal kidney function

As high FGF23 levels lead to a higher risk of developing cardiovascular disease in chronic kidney disease, we next checked the renal function of $Phex^{C733R}$ mice. $Phex^{C733R/Y}$ males and $Phex^{C733R/+}$ females had a similar glomerular filtration rate (GFR) (Figure 2a; Supplementary Figure S4A). Urea and creatinine levels in plasma were also similar between genotypes (Figure 2b and c; Supplementary Figure S4B and C). Moreover, urea clearance showed no differences

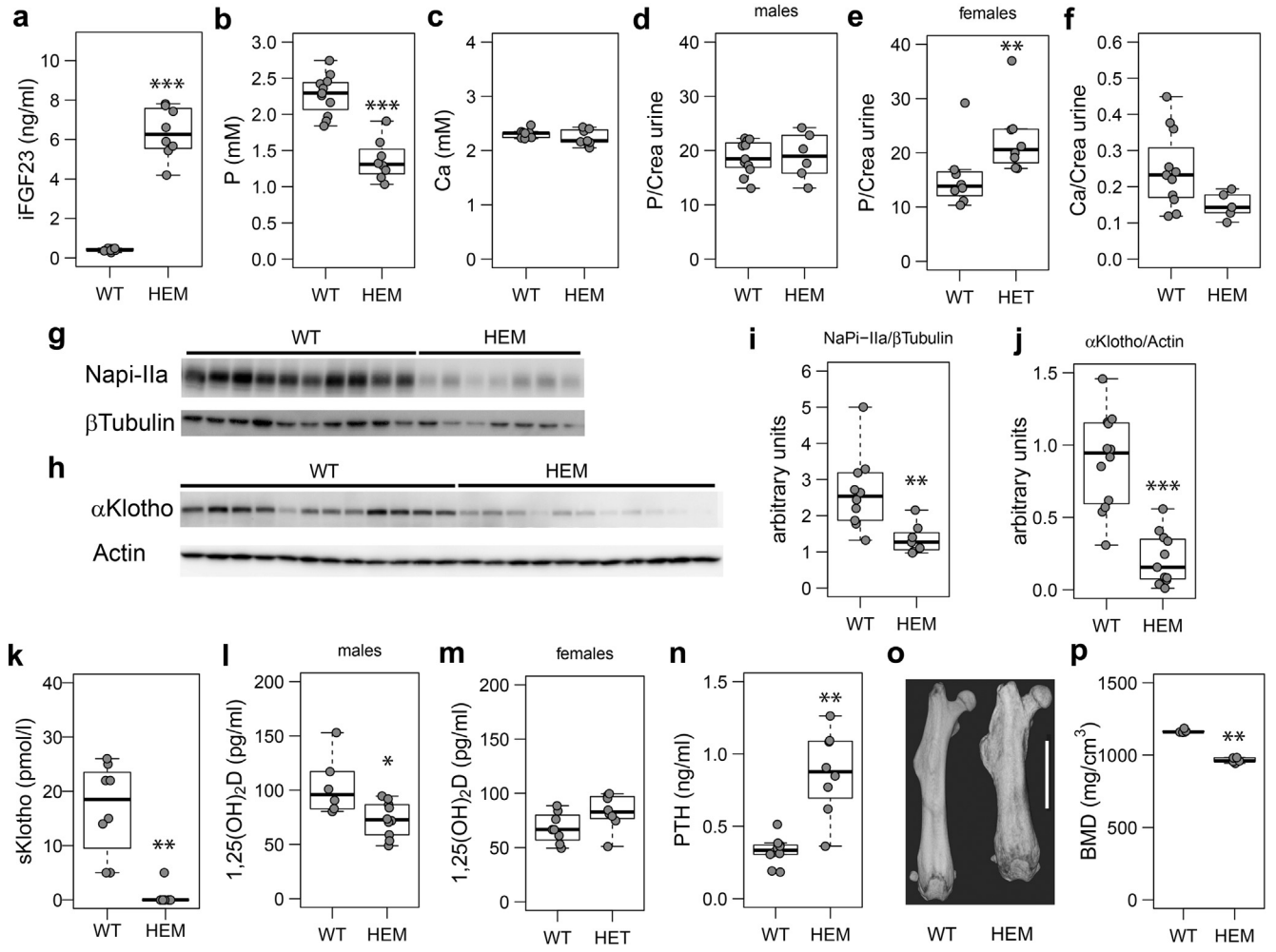

Figure 1 | The *Phex*^{C733R} mouse line is an X-linked hypophosphatemia (XLH) mouse model. (**a**) *Phex*$^{C733R/Y}$ males (HEM) showed significantly higher intact FGF23 circulating levels at 12 weeks of age. (**b,c**) HEM were hypophosphatemic and normocalcemic at 12 weeks of age. (**d**) HEM excreted similar phosphate to creatinine concentration in urine when compared with wild-type (WT) animals at 12 weeks of age. (**e**) *Phex*$^{C733R/+}$ females (HET) were hyperphosphaturic at 12 weeks of age. (**f**) HEM had a tendency to hypocalciuria at 12 weeks of age. (**g**) Representative Western blot image of NaPi-IIa and β-tubulin protein expression in the kidneys of HEM at 12 weeks of age. (**h**) Densitometry analysis showed that NaPi-IIa protein expression normalized to β-tubulin protein expression was significantly reduced in the kidneys of HEM. (**i**) Representative Western blot image of αKlotho and actin protein expression in the kidneys of HEM at 27 weeks of age. (**j**) Densitometry analysis showed that αKlotho protein expression normalized to actin protein expression is significantly reduced in the kidneys of HEM. (**k**) Plasma soluble Klotho is decreased in HEM. (**l**) HEM had lower 1,25(OH)$_2$D levels in plasma at 27 weeks of age. (**m**) HET had similar 1,25(OH)$_2$D levels in plasma at 27 weeks of age. (**n**) HEM showed significantly higher parathyroid (PTH) circulating levels at 12 weeks of age. (**o**) Representative micro computed tomography images of an HEM and a WT male at 27 weeks of age. The HEM animals showed differences in mineralization; the femurs were thicker and shorter. The white scale bar at the right of the image represents 5 mm. (**p**) Bone mineral density (BMD) was assessed by microCT. HEMs had less BMD than WT littermates at 27 weeks of age. Despite otherwise indicated the results presented here have been obtained using male animals; similar results for female animals and older mice are depicted in Supplementary Figure S1 and S2. $n = 7$–12 animals per group. *$P < 0.05$, **$P < 0.01$, ***$P < 0.001$. Ca, calcium; Crea, creatinine; iFGF23, intactFGF23; P, phosphate. To optimize viewing of this image, please see the online version of this article at www.kidney-international.org.

between genotypes (Figure 2d). Periodic acid–Schiff staining showed no apparent histological differences between genotypes, and inflammatory changes were not seen (Figure 2e; Supplementary Table S4). Despite the hyperparathyroidism observed in *Phex*^{C733R} mice, *Phex*$^{C733R/Y}$ animals did not present nephrocalcinosis at 27 weeks of age (Figure 2f).

Phex^{C773R} mice show no evidence for cardiovascular disease

As the CVD risk increases with age, we next studied the effect of primary elevation of FGF23 levels in plasma on indicators of CVD in 27-week-old *Phex*^{C733R} mice. Systolic blood pressure was not increased in these mice; *Phex*$^{C733R/Y}$ males showed lower and *Phex*$^{C733R/+}$ females similar systolic blood pressure compared with their wild-type littermates (Figure 3a and b). *Phex*$^{C733R/Y}$ males and *Phex*$^{C733R/+}$ females showed similar cholesterol and high-density lipoprotein cholesterol levels in blood as compared with their wild-type littermates (Figure 3c and d; Supplementary Figure S5A and B). Moreover, van Kossa staining detected no calcifications in the aorta from both the *Phex*$^{C733R/Y}$ and wild-type males (Figure 3e). As

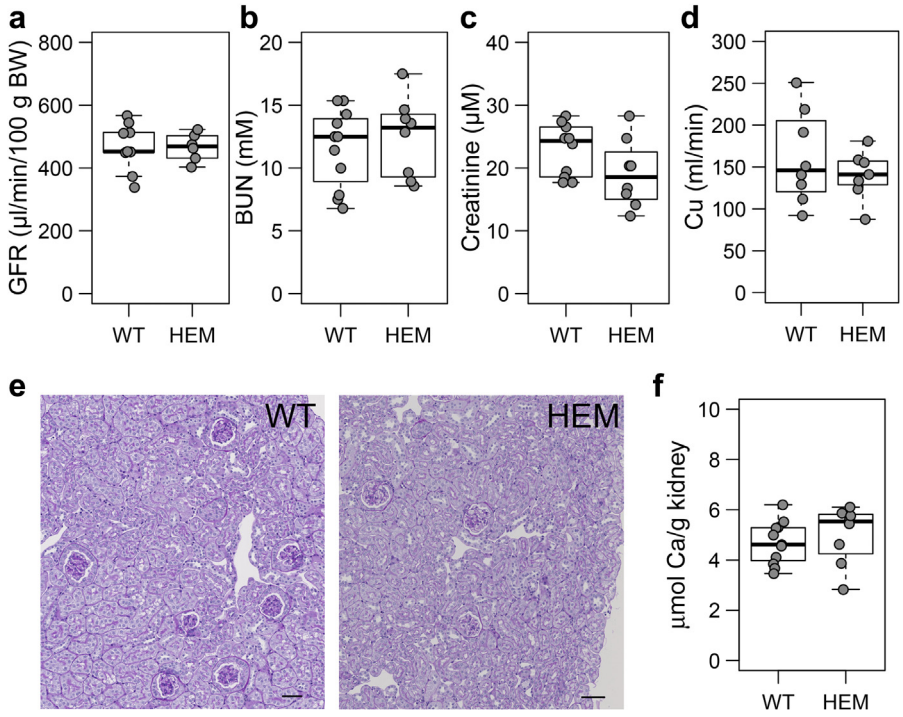

Figure 2 | No renal impairment observed in *Phex*^{C733R} mice. (**a**) The glomerular filtration rate (GFR) was similar between *Phex*$^{C733R/Y}$ males (HEM) and wild-type (WT) littermates at 27 weeks of age. BW, body weight. (**b,c**) Blood urea nitrogen (BUN) and creatinine in plasma were similar between HEM and WT littermates as assessed at 12 weeks of age. (**d**) Urea clearance determined at 27 weeks of age was similar between HEM and WT littermates. (**e**) Representative images of periodic acid–Schiff staining analysis of kidneys from WT and HEM littermates at 27 weeks of age showed no differences between genotypes and no inflammation. Bar = 50 µm. (**f**) The calcium (Ca) content in the kidney was similar between HEM and WT littermates at 27 weeks of age. The results presented here have been obtained using male animals; similar results for female animals are depicted in Supplementary Figure S4. $n = 7$–12 animals per group. Crea, creatinine. To optimize viewing of this image, please see the online version of this article at www.kidney-international.org.

the tibias of the mutant *Phex* mice were shorter, the heart-tibia ratio, a frequently used marker of LVH,[24] is not informative here (Supplementary Table S5). Further markers of left ventricular hypertrophy are an increase in the mRNA expression of atrial natriuretic peptide (*ANP*), brain natriuretic peptide (*BNP*), and β-myosin heavy chain (β*MHC*),[25] and a decrease in medium chain acyl-coA dehydrogenase (*Mcad*). Medium chain acyl-coA dehydrogenase regulates fatty acid oxidation, and a decrease of its levels indicates hypertrophy of cardiomyocyte as they shift their main energy source from fatty acids to glucose.[26] No statistically significant difference in the expression of *Anp*, *Bnp*, and *Mcad* was

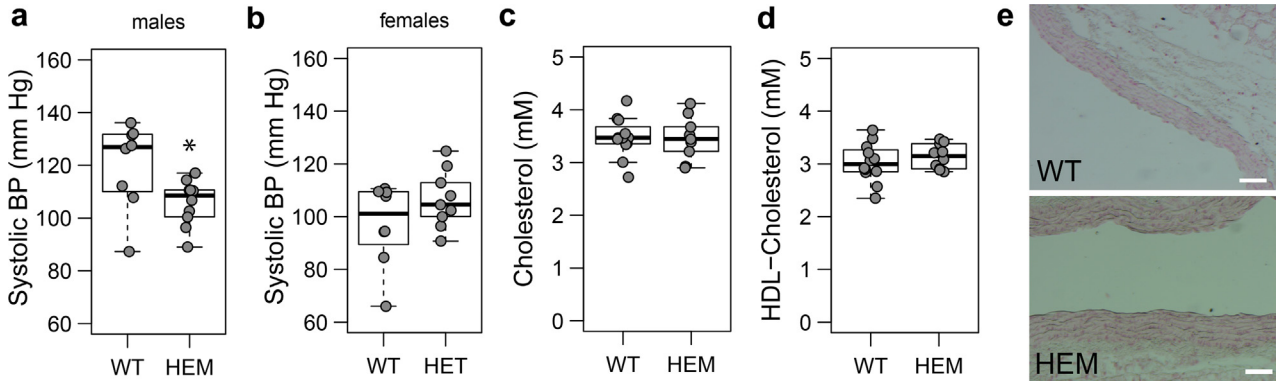

Figure 3 | Blood pressure (BP) and lipid fractions in 27-week-old *Phex*^{C733R} and wild-type (WT) littermates. (**a**) Systolic blood pressure was slightly reduced in *Phex*$^{C733R/Y}$ males (HEM). (**b**) *Phex*$^{C733R/+}$ females (HET) showed similar systolic blood pressure to their WT littermates. (**c,d**) Total and high-density lipoprotein (HDL) cholesterol levels in plasma were similar between HEM and WT littermates. (**e**) Van Kossa staining in the aortic root (magnification x12, bar = 50 µm). HEM and WT showed no calcification in the aorta. The results presented here have been obtained using male animals; similar results for female animals are depicted in Supplementary Figure S5. $n = 8$–10 animals per group in **a–d** and $n = 4$ animals per group in **e**. *$P < 0.05$. To optimize viewing of this image, please see the online version of this article at www.kidney-international.org.

observed in mutant *Phex*$^{C733R/Y}$ males and *Phex*$^{C733R/+}$ females compared with their wild-type littermates (Figure 4a–c; Supplementary Figure S6A–C). β*Mhc* mRNA expression was similar between *Phex*$^{C733R/+}$ and wild-type females, but *Phex*$^{C733R/Y}$ males showed higher β*Mhc* mRNA expression than *Phex*^{WT} males (Figure 4d and e). βMHC has been suggested to be rather a fibrosis instead of an LVH marker;[27] therefore, we next investigated the presence of fibrosis. mRNA levels of the fibrosis markers fibronectin 1 (*Fn1*), TIMP metallopeptidase inhibitor 1 (*Timp1*), collagen type I alpha 1 chain (*Col1a1*), and collagen type III alpha 1 chain (*Col3a1*) revealed no differences between genotypes in male and female animals (Figure 4f–i; Supplementary Figure S6D–G). Histological examination of slides stained with Gomori's blue trichrome did not reveal any fibrotic changes in *Phex*$^{C733R/Y}$ males (Figure 4j; Supplementary Table S4). Transthoracic echocardiography showed that cardiac function (as assessed by ejection fraction and fractional shortening) and left ventricular mass index were comparable among male *Phex*$^{C733R/Y}$ and wild-type littermates (Figure 4k–m). Moreover, left ventricle (LV) anterior and posterior wall thicknesses were similar between the 2 genotypes (Figure 4n). Consistently, morphological analysis of the heart revealed that the left ventricular wall thickness related to the septum thickness was similar between genotypes (Figure 4o and p). Lastly, histological examination of hematoxylin and eosin did not reveal any inflammatory changes (Figure 4o; Supplementary Table S4).

FGFR4 and inflammation in *Phex*^{C773R} mice

FGF23 has been suggested to bind to the FGFR4 in myocytes activating the calcineurin-NFAT pathway and leading to cardiomyopathy.[5,9] *Phex*$^{C733R/Y}$ males showed higher and *Phex*$^{C733R/+}$ females showed similar *Fgfr4* mRNA expression levels compared with wild-type littermates (Figure 5a and b). Yet, in both sexes no increased mRNA expression of the target genes of the calcineurin-NFAT pathway, regulator of calcineurin 1 (*Rcan1*), and transient receptor potential cation channel subfamily C member 6 (*Trpc6*) was observed (Figure 5c and d; Supplementary Figure S7A and B).

CKD is often accompanied by systemic inflammation.[28] A recent report suggested that elevated FGF23 triggers proinflammatory cytokine production in the liver after activating the FGFR4-calcineruin signaling pathway.[29] As in the heart, *Phex*$^{C733R/Y}$ males showed higher *Fgfr4* expression in liver, but the expression of *Rcan1* was significantly decreased in *Phex*$^{C733R/Y}$ males (Figure 5e and f). Moreover, no increased expression of *Trpc6* was observed in *Phex*$^{C733R/Y}$ males' liver tissue (Figure 5g). Additionally we did not observe any inflammatory signs in *Phex*$^{C733R/Y}$ males. *Tnfα*, *Il-6* and *Crp* mRNA expression in liver were similar between the genotypes (Figure 5h–k). C-reactive protein (CRP) in plasma was lower in *Phex*$^{C733R/Y}$ males (Figure 5l). Histological analysis of the liver did not show any cellular infiltration and no morphological differences between genotypes (Figure 5m).

DISCUSSION

FGF23 is highly associated with inflammation, cardiovascular disease, and survival in patients with CKD.[5,29] However, whether FGF23 alone is sufficient to cause inflammation and cardiovascular disease in the absence of kidney disease is an important question and has not been sufficiently addressed to date. Here we used a mouse model for XLH, a disease characterized by a primary increase of intact FGF23. The *Phex*^{C773R} mouse line is a new XLH model. These mice bear a mutation in the coding region for the large extracellular catalytic domain of the PHEX protein, in a highly conserved cysteine residue among other vertebrates, the p.Cys733.[30] Mutations causing changes in the cysteine 733 residue have been also reported in 2 XLH patients.[16,21] As expected, *Phex*^{C773R} mice show high circulating FGF23 levels with values in the nanogram range between 4 and 8 ngl/ml. Like XLH patients,[14] *Phex*^{C773R} mice are hypophosphatemic, normocalcemic, probably hyperphosphaturic and have a tendency to hypocalciuria. As in XLH patients and *Hyp* mice,[14,31] the 1,25(OH)$_2$D levels in *Phex*^{C773R} mice are low despite their hypophosphatemic state. We and others have reported soluble αKlotho as normal in XLH patients.[32,33] Here, in accordance with previous results in *Hyp* mice,[34] the renal expression of αKlotho is reduced in *Phex*^{C773R} mice. Further we observed decreased soluble αKlotho levels. In contrast to *Hyp* mice[35] but in accordance with some XLH patients,[22] these animals present hyperparathyroidism. The *Phex*^{C773R} mice are a very valuable model to address the question of whether primary high circulating FGF23 levels lead to cardiovascular disease, as the mineral-regulating hormone blood levels mimic those in CKD patients: *Phex*^{C733R} mutants have high FGF23 and PTH levels, low 1,25(OH)$_2$D levels, and low soluble αKlotho.[8]

Phex^{C733R} mutants showed normal systolic blood pressure, total and high-density lipoprotein cholesterol levels, and no calcifications in the aorta. Further, we did not observe clear elevations in gene expression of LVH markers and higher incidence of cardiac fibrosis, as observed in previous studies using CKD models, αKlotho-deficient mice, FGF23-injected mice, or normal mice with diet-induced elevation of FGF23.[5,9,10] Moreover, *Phex*^{C733R} mutants did not show left ventricular hypertrophy or altered cardiac function as compared with wild-type littermates. Despite the fact that *Phex*^{C733R} mice have similar or higher FGF23 levels than these models, there are some important differences. These models showed normo- or hyperphosphatemia, whereas the XLH model presented here is hypophosphatemic. Moreover, CKD models and patients display hypertension, circulating uremic toxins, and lipid dysregulation leading to oxidative stress inflammation, problems probably not present in the *Phex*^{C773R} mice. FGF23 mediates cardiomyopathy in CKD probably by binding to FGFR4 in cardiomyocytes.[9] Here we found that although both male and female *Phex*^{C733R} mutant mice have very high circulating FGF23 levels in blood, only *Phex*$^{C733R/Y}$ males showed increased *Fgfr4* mRNA expression in the heart, but with no changes in the mRNA expression of

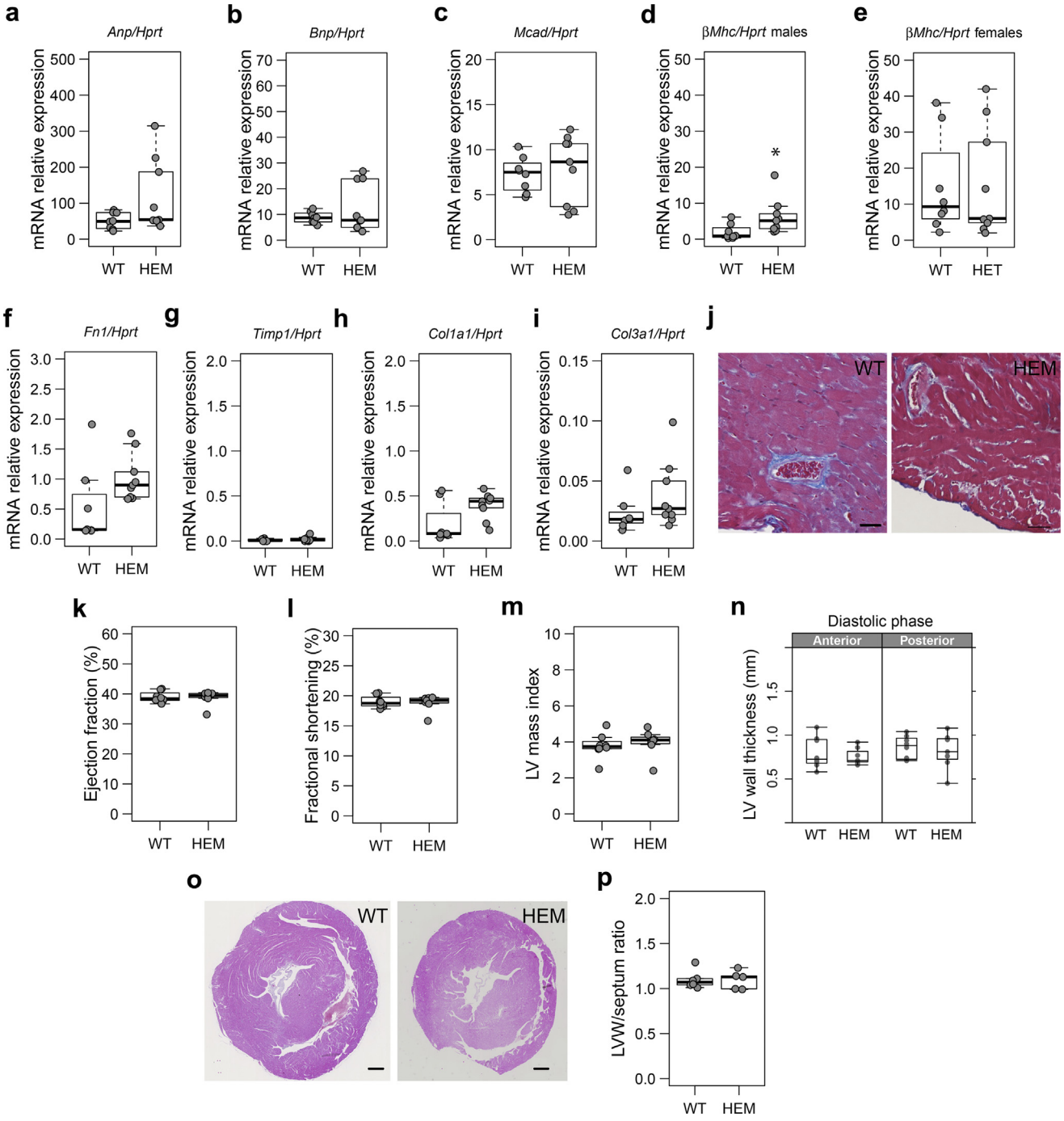

Figure 4 | Assessment of cardiovascular risk factors in the *Phex*^{C733R} mouse line at 27 weeks of age. (**a,b,c**) *Phex*$^{C733R/Y}$ (HEM) and wild-type (WT) males showed similar mRNA expression of the left ventricular hypertrophy (LVH) markers *Anp*, *Bnp,* and *Mcad* in the heart. (**d**) HEM had higher mRNA expression of the LVH marker β*Mhc*. (**e**) *Phex*$^{C733R/+}$ females (HET) showed similar β*Mhc* mRNA expression when compared with their WT littermates. (**f–i**) HEM and WT males showed similar mRNA expression of the fibrotic markers *Fn1*, *Timp1*, *Col1a1*, and *Col3a1* in the heart. (**j**) Representative images of Gomori's blue trichrome staining of hearts from WT and HEM littermates at 27 weeks of age showed no differences in fibrosis appearance between genotypes. Bar = 30 μm. (**k,l**) Transthoracic echocardiography showed similar cardiac function between HEM and WT males as assessed by the ejection fraction and the fractional shortening. (**m,n**) Transthoracic echocardiography showed no LVH between HEM and WT males as assessed by the left ventricle (LV) mass index and the wall thickness during the diastolic phase for the anterior and posterior wall. (**o**) Representative images of hematoxylin and eosin staining analysis of the heart from WT males and HEM littermates at 27 weeks of age showed no differences between genotypes. Bar = 500 μm. (**p**) The left ventricular wall thickness related to the septum thickness was similar between HEM and WT males. $n = 7–10$ animals per group. $^*P < 0.05$. To optimize viewing of this image, please see the online version of this article at www.kidney-international.org.

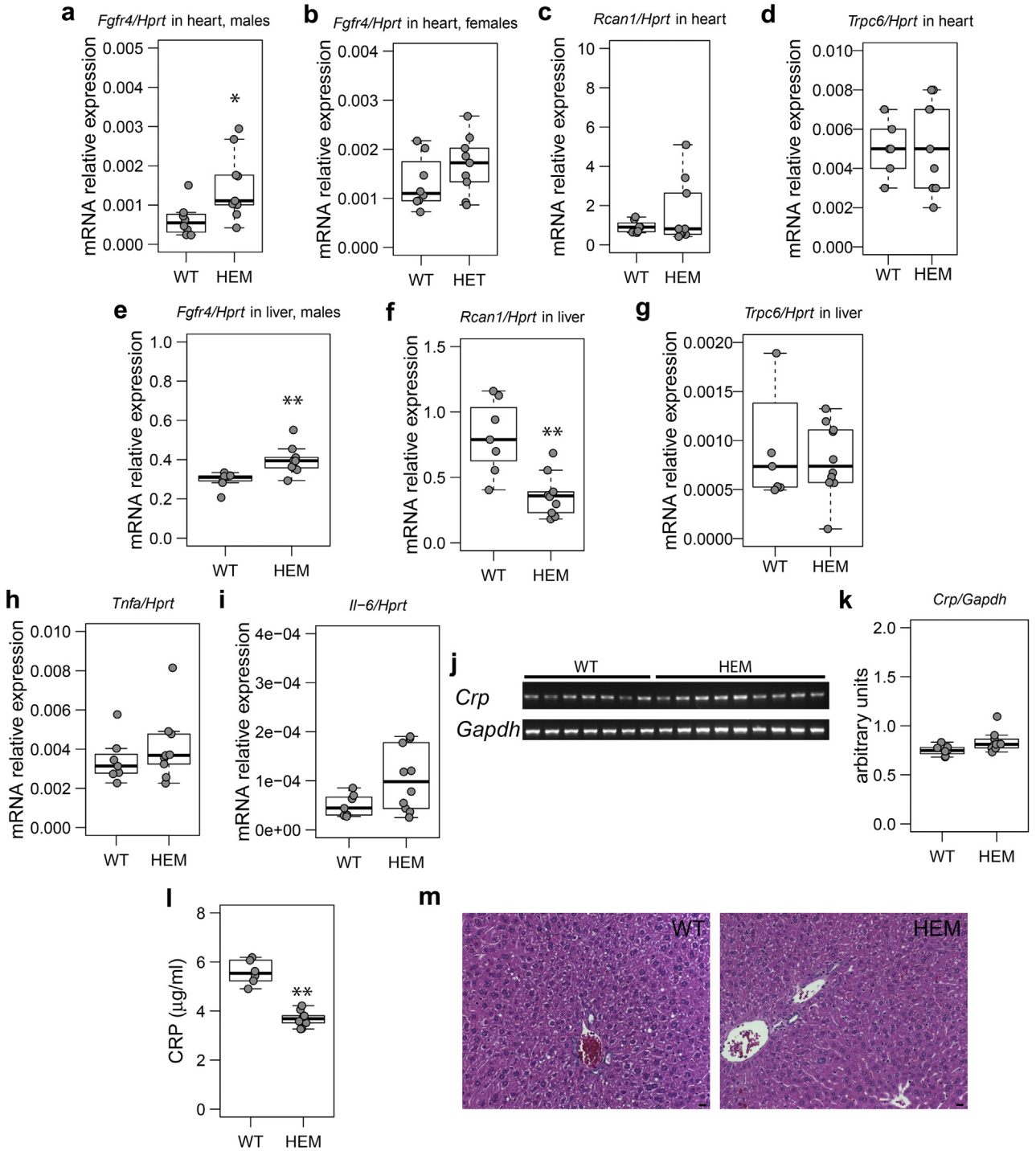

Figure 5 | FGFR4 and inflammation in *Phex*$^{C733R/Y}$ mice at 27 weeks of age. (**a**) *Phex*$^{C733R/Y}$ (HEM) showed higher *Fgfr4* mRNA expression in the heart when compared with wild-type (WT) animals. (**b**) *Phex*$^{C733R/+}$ (HET) and WT females showed similar mRNA expression of *Fgfr4* in the heart. (**c,d**) HEM and WT males showed similar mRNA expression of the target genes of the calcineurin-NFAT pathway *Rcan1* and *Trpc6* in the heart. (**e**) HEM males showed higher *Fgfr4* mRNA expression in the liver when compared with WT animals. (**f**) HEM and WT males showed lower mRNA expression of *Rcan1* in the liver. (**g**) HEM and WT males showed similar mRNA expression of *Trpc6* in the liver. (**h,i**) HEM and WT males had similar mRNA expression of *Tnfα* and *Il-6* in the liver. (**j**) Representative semiquantitative polymerase chain reaction gel of *Crp* and *Gapdh* mRNA expression in the liver of HEM and WT males. (**k**) Densitometry analysis shows that *Crp* mRNA expression normalized to *Gapdh* mRNA expression was similar in the liver from HEM and WT males. (**l**) HEM showed lower circulating C-reactive protein (CRP) levels in plasma when compared with WT animals. (**m**) Representative images of hematoxylin and eosin staining analysis of liver from WT and HEM littermates at 27 weeks of age showed no differences between genotypes. Bar = 20 µm. $n = 7–10$ animals per group. $^*P < 0.05$, $^{**}P < 0.01$. To optimize viewing of this image, please see the online version of this article at www.kidney-international.org.

selected target genes of the calcineurin-NFAT pathway. Moreover, *Fgfr4* mRNA expression was also elevated in the liver of these mice. Yet, this increased *Fgfr4* expression was not associated with a higher expression of selected target genes of the calcineurin-NFAT pathway and of selected cytokines in the liver as reported for FGF23-injected mice and 5/6 nephrectomized rats.[29] Moreover, *Phex*$^{C733R/Y}$ mice appear to have no systemic inflammation because CRP levels in blood were lower and no inflammation signs could be detected in heart, liver, and kidney tissue. Inflammation is commonly accompanying CKD.[28] Yet, a recent prospective study in the Chronic Renal Insufficient Cohort has revealed that high circulating CRP and FGF23 are independent risk factors for mortality in CKD.[36]

Other recent reports also support the hypothesis that elevation of FGF23 *per se* may not be sufficient to cause or modulate left ventricular hypertrophy and other factors are needed. FGF23 has been suggested to have no impact on the appearance of cardiac hypertrophy induced by pressure overload.[37] Moreover, the concerted action of αKlotho and phosphate and probably other factors such as FGF23 has been suggested to contribute to cardiac remodeling in CKD.[10]

Our data confirm a recent report that XLH patients do not develop cardiovascular disease,[38] although another previous publication suggested the opposite.[39] Nehgme *et al.* studied 13 patients (children and young adolescents) treated with vitamin D supplements and phosphate and mild to moderate nephrocalcinosis.[39] Left ventricular hypertrophy was evident in 77%. The nephrocalcinosis in these patients is probably a side effect of the XLH treatment, as in many patients it provokes hyperparathyroidism with the consequent appearance of nephrocalcinosis.[22] In contrast, Takashi *et al.*[38] investigated 24 patients (between 19 and 76 years old) with FGF23-related hypophosphatemic rickets, 10 XLH patients, 2 with autosomal recessive hypophosphatemic rickets 2 (ARHR2) and 13 patients with very high FGF23 levels due to tumor-induced osteomalacia. Except for 2 patients, all were treated with phosphate, vitamin D supplements, or both, and only 4 patients showed estimated GFR levels matching filtration rates observed in patients with CKD. Yet, none of these patients with high circulating FGF23 levels showed any sign of left ventricular hypertrophy. If the presence of renal impairment, differences in vitamin D, and/or phosphate levels is the cause for the differences observed between these human studies remains elusive. Nevertheless, *Phex*^{C733R} mice showed no apparent renal function impairment: the GFR, urea and creatinine in blood, and urea clearance were normal. There were no signs of nephrocalcinosis, and plasma phosphate levels were low.

In conclusion, primary elevation of FGF23 levels *per se* does not cause cardiovascular disease. Probably the most important difference between XLH and CKD patients is the hypophosphatemia in XLH patients in contrast with normo- or hyperphosphatemia found in later stages of CKD. Systemic inflammation may further add to the risk. Our data reinforce previous findings that phosphate levels play a crucial role in pathological cardiac remodeling,[10,40] although its role is probably linked to alteration of other factors. Further differences between XLH and CKD are absence versus presence of a functional PHEX protein, probably absence versus presence of inflammation, probably absence versus presence of uremic toxins, and absence versus presence of renal function impairment. Further studies are required to investigate the synergistic role of FGF23, phosphate, αKlotho, reduced renal function, and systemic inflammation in cardiovascular disease development in CKD.

METHODS

Mice, blood, and organ collection

The *Phex*^{C733RMhda} mouse line was generated within the Munich ENU Mutagenesis Project.[20] For this study *Phex*$^{C733R/+}$ females and *Phex*^{WT} males, backcrossed to the C3Heb/FeJ genetic background for at least 10 generations, were mated. The groups of animals used for analyses are displayed in Supplementary Table S1. At 12 to 13 weeks of age animals were placed in metabolic cages (Tecniplast Inc., Buguggiate, Italy) with a customized standard phosphate diet (0.6% phosphorus, 1% calcium, and 600 IU/kg vitamin D_3; ssniff Spezialdiäten GmbH, Soest, Germany). After 48 hours of adaptation, urine (under mineral oil) and feces were collected during 24 hours, and water consumption, food intake, and body weight were monitored (results in Supplementary Table S2). For blood and organ collection mice were anesthetized with 2% isoflurane prior to collection of blood and killed by cervical dislocation for collection of organs. All procedures applied throughout this study were approved by the Zurich Veterinary Office (Kantonales Veterinäramt) under the reference numbers 05/2013 and 156/2016.

Urine and blood parameters

Creatinine in plasma, creatinine in 24-hour urine, calcium in 24-hour urine and plasma, phosphorus in 24-hour urine and plasma, blood urea nitrogen, urine urea nitrogen, total cholesterol in plasma, and high-density lipoprotein cholesterol was measured in the Zurich Integrative Rodent Physiology (ZIRP) platform of the University of Zurich using the UniCel DxC 800 Synchron System (Beckman Coulter, Brea, CA). Intact FGF23, c-terminal FGF23, PTH, and CRP levels in plasma were quantified by enzyme-linked immunosorbent assay (ELISA) using the FGF23 ELISA Kit (KAINOS, Sissach, Switzerland), the mouse FGF23 (C-Term) ELISA kit (Immunotopics International, San Clemente, CA), the mouse intact PTH ELISA kit (Immunotopics International), and the mouse C-Reactive Protein ELISA kit (Life Diagnostics, West Chester, PA). The $1,25(OH)_2D_3$ levels were determined by radioimmunoassay with the 1,25-Dihydroxy Vitamin D RIA (Immunodiagnostic System, Frankfurt am Main, Germany). Soluble αKlotho was determined by an IP-IB Klotho Assay as described previously[41] at the Physiology Core from the O'Brien Kidney Research Center (UT Southwestern Medical Center, Dallas, TX).

Calcium content in the kidney

Kidneys from males 26 to 28 weeks of age were harvested and decalcified with 1.0 M hydrogen chloride for 60 hours at room temperature.[42] Calcium was determined in the supernatants using the QuantiChrom Calcium assay kit (BioAssay Systems, Hayward, CA). Calcium levels were normalized to the kidney tissue weight.

mRNA analysis by real-time polymerase chain reaction (RT-PCR) and semiquantitative RT-PCR

Isolation of total RNA was performed using the RNeasy Mini Kit (Qiagen, Basel, Switzerland). cDNA was synthesized using the MultiScribe Reverse Transcriptase (Thermo Fisher Scientific, Reinach, Switzerland). RT-PCR was performed with reverse transcript solution, the KAPA Probe Fast qPCR Kit (Kapa Biosystems, Wilmington, MA), and sequence-specific primers and probes on the 7500 Fast Real Time PCR System (Thermo Fisher Scientific). *Cyp27b1* gene expression was detected using the mouse *Cyp27b1* primers from Applied Biosystem (Foster City, CA). The sequences of the primers and probes for the other genes investigated are listed in Supplementary Table S6. Relative expression ratios to *Hprt* were calculated as $2^{\mathrm{Ct}(Hprt)\text{-}\mathrm{Ct}(\text{test gene})}$, where C_t represents the cycle number at a given threshold. Semiquantitative RT-PCR was run to analyze CRP gene expression (*Crp*) following the description by Singh *et al.*[29]

Western blot using renal homogenates and brush border membrane vesicles (BBMV)

BBMV were prepared by an EGTA/Mg^{2+} precipitation method.[43] 20 μg of BBMV or 30 μg renal homogenate was loaded into a 10% polycrylamide gel and transferred electrophoretically, and the blots were incubated with the respective primary antibodies overnight at 4 °C and the corresponding secondary antibodies for 2 hours at room temperature (antibodies listed in Supplementary Table S7). Antibody detection was performed with Immobilon Western Chemiluminescent HRP Substrate (Millipore, Bedford, MA). Images obtained with the Las-4000 Imaging Analysis System (Fujifilm Medical Systems, Stamford, CT) were analyzed with Fiji[44] to calculate the ratio intensity of the protein of interest and the intensity of β-tubulin or actin.

GFR and blood pressure determination

The GFR was measured by a noninvasive-clearance transcutaneous measurement based on the elimination kinetics of a fluorescent exogenous marker, FITC-Sinistrin (Fresenius Kabi, Linz, Austria), in awake mice, using the protocol and devices from NIC-Kidney (Mannheim Pharma & Diagnostic GmbH, Mannheim, Germany).[45,46] Systolic blood pressure was analyzed using the tail-cuff method[47] and the BP-2000 Series II blood pressure analysis system (Visitech Systems, Apex, NC). Blood pressure was measured during 5 consecutive days at the same time during the morning, and only the last day records were taken for analysis.

Micro computed tomography

The Quantum FX microCT Imaging System (PerkinElmer, Waltham, MA) was used for imaging isolated femurs. Whole femur and distal epiphysis were imaged using 20-mm or 5-mm fields of view, respectively, at a tube current of 100 μA, 90 kV tube voltage, and 3-minute scan time. A 1200 mg/cm^3 hydroxy-apatite phantom (Micro-CT HA Phantom, QRM GmbH, Moehrendorf, Germany) was used to translate grayscales into bone mineral density (BMD). BMD and bone volume data was assessed with Analyze 12.0 program (AnalyzeDirect, Inc., Overland Park, KS). BMD was measured from the end of the patellar surface of the distal epiphysis and 100 sections into the diaphysis.

Transthoracic echocardiography

Mice were anesthetized with isoflurane (2-5%)/oxygen (1 L/min) and placed supine on a soft electric warming pad. Temperature was monitored continuously and kept at 37°C. Echocardiographic variables were assessed by using a high-resolution Micro-Ultrasound System (Vevo 3100, Visualsonics FujiFilm). Measurements were obtained from grayscale M-mode and B-mode images, at the mid-papillary level in the parasternal short-axis view. Short-axis M-mode was obtained perpendicular to the midventricular level, confirmed by 2-dimensional echocardiography.[48] Corrected LV mass was calculated considering the specific gravity of cardiac muscle and an intrinsic correction factor.[49] LV internal diastolic diameter as well as anterior and posterior wall thicknesses was measured in the short-axis M-mode view by using the LV trace mode. Three different LV trace measurements were averaged for each animal. All images were analysed by 2 expert operators using the VisualSonics software.

Histology

Calcifications in the aorta were investigated using van Kossa staining.[50] Heart, liver, kidney, aortas, and brain were taken postmortem and fixed in 4% paraformaldehyde for 24 of 48 hours, trimmed, and routinely embedded in paraffin wax. Histological examination was performed from heart, kidney, and liver on hematoxylin and eosin–stained slides by a board-certified veterinary pathologist. Standardized coronal sections of the heart were taken, and the relative thickness of the left ventricular wall was measured. Some heart sections of both genotypes were stained with a trichrome stain (Gomori's blue trichrome) for visualization of connective tissue. Furthermore, periodic acid–Schiff staining of the kidneys was performed.

Statistical analysis

Statistical analysis was performed using R 3.1.2.[51] The Mann-Whitney test was used to test statistical significance between genotypes. Statistical significance was considered at P values < 0.05. Data are represented as means ± SEM.

DISCLOSURE

All the authors declared no competing interests.

ACKNOWLEDGMENTS

The study was supported in part by the Swiss National Center for Competence in Research NCCR Kidney. CH funded by the Swiss National Science Foundation. FP and GGC are the recipients of a Sheikh Khalifa's Foundation Assistant Professorship in Cardiovascular Regenerative Medicine and Vascular Biology at the Faculty of Medicine, University of Zürich. SC is supported by the Holcim Foundation. We thank Prof. Orson Moe and the O'Brien Kidney Research Center at the University of Texas Southwestern Medical Center P30-DK079328 for their help with the soluble Klotho determination in plasma. We kindly thank Prof. Fernando Santos (University of Oviedo, Spain) for his comments about XLH and hypophosphatemia diseases, Prof. Susanne Ulbrich and Alba Rudolf Vegas (ETH, Switzerland) for helping with sections imaging, and Dr. Nati Hernando (University of Zurich, Switzerland) for the fruitful discussions. We gratefully thank Dr. Svende Pfundstein for helping with the FITC-sinistrin tail injections, Dr. Petra Seebeck for helping with the bone imaging, Dr. Alexander Akhmendov for helping with the organization of the echocardiography experiments, Claudia Meyer for helping with the tissue processing and staining, and Udo Schnitzbauer for technical support at the University of Zurich (Switzerland). The authors gratefully thank Sandra Hoffmann from the Helmholtz Center in Munich (Germany) for the organization of the animal shipment. The use of the ZIRP Core facility for Rodent Phenotyping and the Histology Laboratory at the University of Zurich is also acknowledged.

SUPPLEMENTARY MATERIAL

Figure S1. *Phex*$^{C733R/+}$ female mice are an X-linked hypophosphatemia mouse model. (**A**) *Phex*$^{C733R/+}$ females (HET) show significantly higher intact FGF23 circulating levels when compared with their wild-type (WT) female counterparts. (**B**) HET are hypophosphatemic when compared with their WT female counterparts. (**C**) HET are normocalcemic as XLH patients. (**D**) Representative Western blot image of NaPi-IIa and actin protein expression in the kidneys of HET at 12 weeks of age. (**E**) Densitometry analysis showed that NaPi-IIa protein expression normalized to actin protein expression was significantly reduced in the kidneys of HET. (**F**) HET show a tendency to excrete less calcium in urine ($P = 0.07$). (**G**) HET have high PTH levels in plasma when compared with WT females. $n = 8$–9 animals per group. $^{*}P < 0.05$, $^{***}P < 0.001$.

Figure S2. The *Phex*^{C733RMhda} mouse line is an X-linked hypophosphatemia mouse model. (**A,B**) Both *Phex*$^{C733R/Y}$ males (HEM) and *Phex*$^{C733R/+}$ females (HET) show significantly higher intact FGF23 circulating levels when compared with their wild-type (WT) counterparts at 27 weeks of age. (**C**) HEM show significantly higher C-terminal FGF23 circulating levels when compared with their WT counterparts at 27 weeks of age. (**D–G**) HEM and HET are hypophosphatemic and normocalcemic when compared with WT animals at 27 weeks of age. $n = 7$–12 animals per group. $^{***}P < 0.001$.

Figure S3. Expression of metabolizing enzymes of 1,25$(OH)_2$ Vitamin D in the *Phex*^{C733RMhda} mouse line at 27 weeks of age. (**A**) *Phex*$^{C733R/Y}$ males (HEM) have lower *Cyp27b1* mRNA expression normalized to *Hprt* mRNA expression when compared with wild-type (WT) male littermates. (**B**) Representative Western blot image of Cyp24a1 and actin protein expression in the kidneys of HEM compared with WT males. (**C**) Densitometry analysis of the Western blot image in S2B shows that Cyp24a1 protein expression normalized to actin protein expression is significantly higher in the kidneys of HEM when compared with WT males. (**D**) *Phex*$^{C733R/+}$ females (HET) have similar *Cyp27b1* mRNA expression normalized to *Hprt* mRNA expression when compared with WT female littermates. (**E**) Representative Western blot image of Cyp24a1 and actin protein expression in the kidneys of HET compared with WT females. (**F**) Densitometry analysis of the Western blot image in 2e shows that Cyp24a1 protein expression normalized to actin protein expression is similar in the kidneys of HET when compared with WT females. $n = 7$–12 animals per group. $^{*}P < 0.05$, $^{**}P < 0.01$.

Figure S4. No renal impairment observed in *Phex*$^{C733R/+}$ female mice. (**A**) The glomerular filtration rate (GFR) was similar between *Phex*$^{C733R/+}$ females (HET) and wild-type (WT) littermates at 27 weeks of age. (**B,C**) Blood urea nitrogen (BUN) and creatinine in plasma were similar between HET and WT littermates as assessed at 12 weeks of age. $n = 8$–10 animals per group.

Figure S5. Total and HDL cholesterol in *Phex*$^{C733R/+}$ female mice compared with *Phex*^{WT} female mice. (**A,B**) *Phex*$^{C733R/+}$ females (HET) showed similar cholesterol and high-density lipoprotein cholesterol levels compared with their wild-type (WT) female littermates. $n = 8$–10 animals per group.

Figure S6. Assessment of cardiovascular risk factors in *Phex*$^{C733R/+}$ female mice at 27 weeks of age. (**A–C**) *Phex*$^{C733R/+}$ females (HET) and wild-type (WT) females showed similar mRNA expression of the left ventricular hypertrophy (LVH) markers *Anp*, *Bnp* and *Mcad* in the heart. (**D–G**) HET and WT females showed similar mRNA expression of the fibrotic markers *Fn1, Timp1, Col1a1,* and *Col3a1* in the heart. $n = 8$–10 animals per group.

Figure S7. mRNA expression of selected target gene of the calcinurin-NAFT pathway in *Phex*$^{C733R/+}$ female mice at 27 weeks of age. *Phex*$^{C733R/Y}$ (HEM) and wild-type (WT) males showed similar mRNA expression of the target genes of the calcineurin-NAFT pathway (**A,B**) *Rcan1* and (**C,D**) *Trpc6* in the heart. $n = 8$–9 animals per group.

Table S1. Age at sacrifice, body weight, number of animals, and analysis performed in each experimental group.

Table S2. Metabolic parameters of *Phex* mutant mice.

Table S3. Bone parameters obtained by micro computed tomography from bones of *Phex* mutant and wild-type mice.

Table S4. Histological data from heart, liver, and kidneys of *Phex* mutant and wild-type mice.

Table S5. The marker of left ventricular hypertrophy heart-tibia ratio is not informative in *Phex* mutant mice.

Table S6. Primers and probes for real-time polymerase chain reaction.

Table S7. Antibodies for Western Blot.

Supplementary References.

Supplementary material is linked to the online version of the paper at www.kidney-international.org.

REFERENCES

1. Go A, Chertow G, Fan D, et al. Chronic kidney disease and the risks of death, cardiovascular events, and hospitalization. *New Engl J Med*. 2004;351:1296–1305.
2. Alhaj E, Alhaj N, Rahman I, et al. Uremic cardiomyopathy: an underdiagnosed disease. *Conges Heart Fail*. 2013;19:E40–E45.
3. Paoletti E, Bellino D, Cassottana P, et al. Left ventricular hypertrophy in nondiabetic predialysis CKD. *Am J Kidney Dis*. 2005;46:320–327.
4. Levy D. Prognostic implications of echocardiographically determined left ventricular mass in the Framingham Heart Study. *New Engl J Med*. 1990;322:1561–1566.
5. Faul C, Amaral AP, Oskouei B, et al. FGF23 induces left ventricular hypertrophy. *J Clin Invest*. 2011;121:4393–4408.
6. Bergwitz C, Jüppner H. Regulation of phosphate homeostasis by PTH, vitamin D, and FGF23. *Ann Rev Med*. 2010;61:91–104.
7. Hu M, Shiizaki K, Kuro-o M, et al. Fibroblast growth factor 23 and Klotho: physiology and pathophysiology of an endocrine network of mineral metabolism. *Ann Rev Physiol*. 2013;75:503–533.
8. Kuro-o M, Kuro-o M. Klotho and the aging process. *Korean J Int Med*. 2011;26:113–122.
9. Grabner A, Amaral AP, Schramm K, et al. Activation of cardiac fibroblast growth factor receptor 4 causes left ventricular hypertrophy. *Cell Metab*. 2015;22:1020–1032.
10. Hu MC, Shi M, Cho HJ, et al. Klotho and phosphate are modulators of pathologic uremic cardiac remodeling. *J Am Soc Nephrol*. 2015;26:1290–1302.
11. Isakova T, Wahl P, Vargas GS, et al. Fibroblast growth factor 23 is elevated before parathyroid hormone and phosphate in chronic kidney disease. *Kidney Int*. 2011;79:1370–1378.
12. Jonsson KB, Zahradnik R, Larsson T, et al. Fibroblast growth factor 23 in oncogenic osteomalacia and X-linked hypophosphatemia. *New Engl J Med*. 2003;348:1656–1663.
13. Blau JE, Collins MT. The PTH-Vitamin D-FGF23 axis. *Rev Endocr Metab Disord*. 2015;16:165–174.
14. Santos F, Fuente R, Mejia N, et al. Hypophosphatemia and growth. *Pediatr Nephrol*. 2013;28:595–603.
15. Francis F, Hennig S, Korn B, et al. A gene (PEX) with homologies to endopeptidases is mutated in patients with X-linked hypophosphatemic rickets. The HYP Consortium. *Nat Genet*. 1995;11:130–136.
16. Filisetti D, Ostermann G, von Bredow M, et al. Non-random distribution of mutations in the PHEX gene, and under-detected missense mutations at non-conserved residues. *Eur J Hum Genet*. 1999;7:615–619.
17. Lorenz-Depiereux B, Guido VE, Johnson KR, et al. New intragenic deletions in the Phex gene clarify X-linked hypophosphatemia-related abnormalities in mice. *Mamm Genome*. 2004;15:151–161.
18. Yuan B, Takaiwa M, Clemens TL, et al. Aberrant Phex function in osteoblasts and osteocytes alone underlies murine X-linked hypophosphatemia. *J Clin Invest*. 2008;118:722–734.
19. Eicher EM, Southard JL, Scriver CR, et al. Hypophosphatemia: mouse model for human familial hypophosphatemic (vitamin D-resistant) rickets. *Proc Nat Acad Sci U S A*. 1976;73:4667–4671.

20. Sabrautzki S, Rubio-Aliaga I, Hans W, et al. New mouse models for metabolic bone diseases generated by genome-wide ENU mutagenesis. *Mamm Genome*. 2012;23:416–430.
21. Tyynismaa H. Identification of fifteen novel PHEX gene mutations in Finnish patients with hypophosphatemic rickets. *Hum Mutat*. 2000;15:383–384.
22. Schmitt CP, Mehls O. The enigma of hyperparathyroidism in hypophosphatemic rickets. *Pediatr Nephrol*. 2004;19:473–477.
23. Cheung M, Roschger P, Klaushofer K, et al. Cortical and trabecular bone density in X-linked hypophosphatemic rickets. *J Clinic Endocrinol Metab*. 2013;98:E954–E961.
24. Yin FC, Spurgeon HA, Rakusan K, et al. Use of tibial length to quantify cardiac hypertrophy: application in the aging rat. *Am J Physiol*. 1982;243:H941–H947.
25. Dorn GW 2nd, Robbins J, Sugden PH. Phenotyping hypertrophy: eschew obfuscation. *Circ Res*. 2003;92:1171–1175.
26. Rimbaud S, Garnier A, Ventura-Clapier R. Mitochondrial biogenesis in cardiac pathophysiology. *Pharmacol Rep*. 2009;61:131–138.
27. Pandya K, Kim HS, Smithies O. Fibrosis, not cell size, delineates beta-myosin heavy chain reexpression during cardiac hypertrophy and normal aging in vivo. *Proc Nat Acad Sci U S A*. 2006;103:16864–16869.
28. Castillo Rodríguez E, Pizarro Sánchez S, Sanz A, et al. Inflammatory Cytokines as Uremic Toxins: "Ni Son Todos Los Que Estan, Ni Estan Todos Los Que Son". *Toxins*. 2017;9:114.
29. Singh S, Grabner A, Yanucil C, et al. Fibroblast growth factor 23 directly targets hepatocytes to promote inflammation in chronic kidney disease. *Kidney Int*. 2016;90:985–996.
30. Du L, Desbarats M, Viel J, et al. cDNA cloning of the murine Pex gene implicated in X-linked hypophosphatemia and evidence for expression in bone. *Genomics*. 1996;36:22–28.
31. Tenenhouse HS. Molecular basis of renal disease. X-linked hypophosphataemia: a homologous disorder in humans and mice. *Nephrol Dial, Transplant*. 1999;14:333–341.
32. Carpenter TO, Insogna KL, Zhang JH, et al. Circulating levels of soluble klotho and FGF23 in X-linked hypophosphatemia: circadian variance, effects of treatment, and relationship to parathyroid status. *J Clinic Endocrinol Metab*. 2010;95:E352–E357.
33. Pavik I, Jaeger P, Ebner L, et al. Soluble klotho and autosomal dominant polycystic kidney disease. *Clin J Am Soc Nephrol*. 2012;7:248–257.
34. Farrow EG, Summers LJ, Schiavi SC, et al. Altered renal FGF23-mediated activity involving MAPK and Wnt: effects of the Hyp mutation. *J Endocrinol*. 2010;207:67–75.
35. Tenenhouse HS. X-linked hypophosphataemia: a homologous disorder in humans and mice. *Nephrol Dial Transplant*. 1999;14:333–341.
36. Munoz Mendoza J, Isakova T, Cai X, et al. Inflammation and elevated levels of fibroblast growth factor 23 are independent risk factors for death in chronic kidney disease. *Kidney Int*. 2017;91:711–719.
37. Slavic S, Ford K, Modert M, et al. Genetic ablation of Fgf23 or Klotho does not modulate experimental heart hypertrophy induced by pressure overload. *Sci Rep*. 2017;7:11298.
38. Takashi Y, Kinoshita Y, Hori M, et al. Patients with FGF23-related hypophosphatemic rickets/osteomalacia do not present with left ventricular hypertrophy. *Endocr Res*. 2016:1–6.
39. Nehgme R, Fahey JT, Smith C, et al. Cardiovascular abnormalities in patients with X-linked hypophosphatemia. *J Clin Endocrinol Metab*. 1997;82:2450–2454.
40. Tonelli M, Sacks F, Pfeffer M, et al. Relation between serum phosphate level and cardiovascular event rate in people with coronary disease. *Circulation*. 2005;112:2627–2633.
41. Barker S, Pastor J, Carranza D, et al. The demonstration of αKlotho deficiency in human chronic kidney disease with a novel synthetic antibody. *Nephrol Dial Transplant*. 2015;30:223–233.
42. Li Q, Chou D, Price T, et al. Genetic modulation of nephrocalcinosis in mouse models of ectopic mineralization: the Abcc6^{tm1Jfk} and Enpp1^{asj} mutant mice. *Lab Invest*. 2014;94:623–632.
43. Biber J, Stange G, Stieger B, et al. Transport of L-cystine by rat renal brush border membrane vesicles. *Pflugers Arch*. 1983;396:335–341.
44. Schindelin J, Arganda-Carreras I, Frise E, et al. Fiji: an open-source platform for biological-image analysis. *Nat Methods*. 2012;9:676–682.
45. Schreiber A, Shulhevich Y, Geraci S, et al. Transcutaneous measurement of renal function in conscious mice. *Am J Physiol Renal Physiol*. 2012;303:F783–F788.
46. Schock Kusch D. Reliability of transcutaneous measurement of renal function in various strains of conscious mice. *PloS One*. 2013;8:e71519.
47. Zhao X, Ho D, Gao S, et al. Arterial pressure monitoring in mice. *Curr Protoc Mouse Biol*. 2011;1:105–122.
48. Reynolds JO, Quick AP, Wang Q, et al. Junctophilin-2 gene therapy rescues heart failure by normalizing RyR2-mediated Ca2+ release. *Int J Cardiol*. 2016;255:371–380.
49. Respress JL, Wehrens XH. Transthoracic echocardiography in mice. *J Vis Exp*. 2010;39.
50. Mulisch M, Welsch U. *Romeis - Mikroskopische Technik*, 19 edn. Springer Spektrum, 2015.
51. *Team RC: R: A language and environment for statistical computing* [computer program]. Vienna, Austria: R Foundation for Statistical Computing; 2014.